Zinc Ion Stress and Photo-radical Redox Stress Mechanisms of ZnO nanoparticle toxicity to *Escherichia coli* K12 enhanced by the nano-bio interface

JONATHAN MCQUILLAN[1] and ANDREW M. SHAW[1]

[1]Biosciences, College of Life and Environmental Sciences, University of Exeter, Exeter, EX4 4QD, UK

Correspondence: Dr Andrew M. Shaw, Biosciences, College of Life and Environmental Sciences, University of Exeter, Exeter, EX4 4QD, UK. Email: andrew.m.shaw@exeter.ac.uk Phone: +441392263495. Fax: +441392263434.

Two toxicity mechanisms for ZnO nanoparticles to *E. coli* K12 have been studied: Zn^{2+} metal stress following the dissolution of the ZnO nanoparticle at the membrane boundary; and photo-radical-induced redox stress following photo-electron generation at the nanoparticle surface under ultraviolet radiation. The rate of ZnO nanoparticle dissolution has been measured using Inductively Coupled Plasma Mass Spectrometry. Genes whose products control the flux of Zn^{2+} across the cell membrane showed an enhanced regulation when delivered by the nanoparticle compared with that from solution as Zn^{2+} chloride. The photo-radical induced stress response did not show superoxide dismutase encoding gene regulation but did show photo-enhanced redox stress in the metabolism. In each case the role of the nano-bio interface is discussed in the explanation of concentration enhancement and radical species diversification. The two stress mechanisms have shown clear speciation in the mechanisms of nanoparticle toxicity judged by physical and genetic stress responses.

Keywords: ZnO nanoparticles, nano-bio interface, dissolution, stress response, photo-radical

Introduction

Zinc oxide nanoparticles are produced at a rate of approximately 10^3 tonnes annually for incorporation into sunscreen and cosmetics, and will ultimately end up in the environment with potential toxicological effects [1]. For example these materials have well known anti-bacterial properties and have been incorporated into anti-bacterial fabrics [2] and orthopaedic cements [3-5] with efficacy against Gram negative and Gram positive organisms [6-12].

The physical chemistry properties of the nano-bio interface control the mechanisms of toxicity. Principally, the proximal association of the particles to the target cells, potentially the shape, the native surface chemistry of the particles and any subsequent modification of the surface with protein corona all contribute to the ultimate toxicity in biological systems [13]. There are two toxicological mechanisms proposed for ZnO nanoparticles: one is nanoparticle dissolution to release Zn^{2+} and the second is the photo-production of radicals which induce radical stress. ZnO nanoparticle dissolution is favoured by a high active surface area and the subsequent delivery of the Zn^{2+} proximal to the membrane or cell surface. The zinc ion is an essential co-factor in all 6 functional classes of enzymes [14-20] but at high concentrations it may compete with di-valent ion biding sites on proteins, leading to toxicity, and therefore Zn^{2+} is subject to active homeostasis. The other mechanism is the production of photo-electrons and photo-radicals at the nanoparticle surfaces under ultra violet light at wavelengths shorter than approximately 380 nm, which corresponds in energy to the material band gap of 3.37 eV. Photo-radicals produced from ZnO have been used for the reduction of organics in water [21] and are known to degrade redox dyes methylene orange [22] and methylene blue [23]. The primary toxicity concern is the large-scale use of nanomaterials in sunscreen where transport of Zn from ZnO nanoparticles, across the dermal layers into the blood, has been proven definitively [24]. It is then evident that extended exposure to ZnO nanoparticles will induce a toxic response in the skin flora resulting from both the photo-chemical activation of the nanoparticles inducing redox stress and the dissolution of the nanoparticles inducing and adaptive metal stress response.

For the Zn^{2+}-based metal stress mechanism, the key physical parameter for toxicity is the rate of dissolution leading to the accumulation of zinc ions within the formulation of a sunscreen on the skin surface or experimentally in a culture medium. If the concentration is sub-lethal then the bacterium can mount a successful adaptive stress response, which modulates the flux of metal ions across the cell wall to maintain the optimal concentration in the cytosol, resulting in cell survival. For this study the model Gram negative bacterium is *Escherichia coli* K12 which controls intracellular zinc by regulating the levels of Zn^{2+} transport proteins by up-regulating the corresponding genetic transcripts. The primary Zn^{2+} importer in *E. coli* is an ABC (ATP-binding cassette) family member [25], ZnuABC [26, 27],

which is regulated through the activity of the Zinc Uptake Regulator (Zur), a Fur family member transcription factor [28, 29]. The primary Zn^{2+} exporter is a P-Type ATPase, ZntA [30-33] which is regulated through the activity of ZntR, a MerR family member [34-36]. The genes are inversely regulated in response to femtomolar changes in the free Zn^{2+} concentration in the cytosol [28].

Similarly, *E. coli* can adapt to photo-radical stress by increasing the level of transcription for genes encoding various systems for neutralising radicals and their effects in the cell. The OxyR and SoxR proteins are redox-dependant protein switches that regulate the expression of genes to counteract oxidative stress in response to hydrogen peroxide or superoxide radicals respectively. The OxyR protein is synthesised constitutively in the cytosol and forms an inactive tetramer. In response to H_2O_2 the complex undergoes structural re-arrangement through inter-molecular di-sulphide bond formation between redox active cysteine residues [37, 38]. The active complex may regulate the expression of at least 32 genes including *katG*; a homo-tetrameric enzyme that catalyses breakdown of hydrogen peroxide [39]. SoxR is activated by superoxide after oxidation of redox-sensitive Fe-S clusters. Active SoxR promotes transcription of a second transcription factor, SoxS, which may regulate the expression of up to 47 genes, including anti-oxidant systems such as the superoxide dismutases, which catalyse the dismutation of the superoxide radical [40].

In this study, we investigate the dual ZnO nanoparticle toxicity mechanisms against *E. coli* K12. Nanoparticle dissolution was measured in the minimal salts culture medium by ultracentrifugation followed by determining total Zn by Inductively Coupled Plasma Mass Spectrometry. Photo-radical generation properties were investigated following photo-electron production leading to a colour change in the redox dye 2, 6-dichloroindolphenol (DCPIP). This simple assay allows zinc speciation; the presence of photo-electrons requires a nanoparticle band gap and therefore ZnO must be present as the nanoparticle. Both dissolution and photo-radical generation are toxic to the bacterium and activate stress responses against excess zinc ions and against free radicals, which were measured quantitatively using real-time PCR of targeted gene panels for each adaptive response. The differential toxicity and mechanisms of nano-bacterial interaction are discussed.

Methods

Nanoparticle characterisation

Zinc oxide nanoparticles (Z-COTE®) were purchased from BASF. The nanoparticles had a mean diameter of 150 ± 60 nm (mean ± SD) measured in TEM images and a surface area determined by BET isotherm of 12-14 m^2 g^{-1}. Analysis of the nanopowder under SEM coupled to an EDAX detector confirmed that the nanoparticles were ZnO with no other elements detected.

Bacterial culture

Escherichia coli K12 (MG1655) was cultured in Neidhardt's minimal salts medium with 0.1% (w/v) glucose. For exposure to zinc, exponentially growing cultures of *E. coli* were mixed 1:1 with sterile minimal salts medium containing zinc oxide nanoparticles or zinc chloride. All culture steps were performed aerobically at 37^{o}C and viable cell numbers were determined by measuring colony forming units (CFUs) on Lauria agar.

ZnO nanoparticle dissolution

Dissolution measurements were made using Inductively Coupled Plasma Mass Spectrometry (ICP-MS) following ultracentrifugation of ZnO nanoparticle dispersions. The zinc oxide nanoparticles were suspended in the minimal salts medium at a concentration of100 µg mL^{-1}. Subsequently, the zinc oxide nanoparticles were removed from suspension by ultracentrifugation (50,000 × *g*, 30 minutes, Beckmann-Coulter) over the time course 0 hrs, 1hr, 2 hrs, 3hrs and 4 hrs. A 200 mg aliquot of each supernatant was mixed with 1 mL of a 1:1 mixture of nitric acid and hydrogen peroxide, and microwave digested. The digests were made up to 5 g with ultrapure water and measured with ICP-MS in standard analysis mode (7500 ICP-MS, Agilent). Total Zn concentration in the samples was determined by measuring the isotopes ^{64}Zn, ^{67}Zn, ^{68}Zn and ^{69}Zn. Quantification was performed by external calibration using Zn standard solutions and ^{103}Rh as an internal standard, correcting each sample for a procedural blank. The experiment was carried out twice, and each sample was prepared in triplicate and measured 5 times.

Photo-toxic effects

Photo-electron production from the ZnO nanoparticles was measured by monitoring the absorbance change at 595 nm of the redox sensitive dye, 2,6-dichlorophenolindolphenol (DCPIP). A suspension of ZnO nanoparticles in the minimal salts medium was mixed with an aqueous solution of DCPIP to a final concentration of 1 mM. The mixture was either kept in the dark or irradiated with 375 ± 5 nm light from a lid-mounted LED (NICHIA, Japan) producing a power of 2 mW. To determine potential photo-toxic effects of the ZnO nanoparticles, exponentially replicating *E. coli* were harvested by centrifugation (5,000 x *g*, 5 minutes) and mixed with a suspension of the ZnO nanoparticles in deionised water at a density of 10^6 CFU mL^{-1}. The suspensions were irradiated with 375 nm light from the LED or kept in the dark. Bacterial survival was measured by CFUs compared to the appropriate control; either *E. coli* in water in the dark or *E. coli* in water with 375 nm light.

Real-time PCR

Gene regulation was measured using real-time PCR. Exponentially replicating *E. coli* in the minimal salts medium were mixed 1:1 with sterile medium containing a suspension of the ZnO nanoparticles (100 µg mL^{-1}) or Zinc Chloride (10 µg mL^{-1}). The ZnO nanoparticle treated bacteria were kept in the dark or irradiated with 375 nm light. The abundance of specific mRNA sequences in the total RNA extracted from the suspensions was compared to untreated controls, which were *E. coli* in unmodified minimal salts medium in the dark.

Total RNA was isolated from exponentially dividing *E. coli* using the RNA Protect Bacterial Reagent and the RNeasy Mini Kit (Qiagen). Residual DNA was removed from RNA samples by digesting with RNase-free DNase (RQ1, Promega) and RNA was purified using the RNeasy Clean-up Protocol. First strand cDNA synthesis was performed using the Thermoscript system (Invitrogen) and random hexamer primers. Real time PCR was performed to determine the relative abundance of specific mRNA sequences using the Stratagene MxPro system and the SYBR green DNA detection chemistry (Biorad). All RT-PCR reactions were performed in duplicate and each experiment was repeated at least twice. Data were analysed according to the method of Pfaffl (38), using a dilution series based on pooled cDNA samples to determine the primer efficiency. The internal reference gene was *rrsB* as used by others in metal stress measurements for *E. coli*. Primer sequences are provided in the supporting information, Table S1.

Transmission Electron Microscopy

Suspensions of E. coli cells and ZnO nanoparticles in the minimum salts medium were gently agitated for 30 minutes. Subsequently, 2 μL samples were dried onto Cu-Formvar TEM grids. The bacterial were fixed by resting the grids on droplets of 1% (v/v) glutaraldehyde for 10 minutes and washed 10 times on droplets of deionised water. Images were acquired on a JEOL 1400 TEM at an accelerating voltage of 80 KeV.

Results

We used commercially available Z-COTE® ZnO nanoparticles to investigate the effect of nanoparticle dissolution and radical generation in ultraviolet light on *E. coli* K12. For nanoparticle suspensions in the minimal salts medium we measured a large size distribution (150 ± 60 nm; mean ± SD) and irregular, polyhedral shapes in TEM images. Suspensions of ZnO nanoparticles and *E. coli* were examined in TEM imaging studies by adopting a minimal specimen preparation lacking embedding and sectioning procedures to show clearly the nanoparticle-membrane interaction. Images appeared as shown in Figure 1(a) for suspensions of the nanoparticles in a minimal salts medium although it is not clear that the aggregation does not occur during the drying process. Similar aggregation clusters are seen in association with the bacterium Figure 1(b), with the same caveat about the origin of the aggregation process.

The minimal salts medium supported *E. coli* growth and replication and allowed a stable nanoparticle dispersion. The minimal salts medium has a background concentration of 0.227 μg g^{-1} of Zn^{2+} in the bulk solution phase, rising to 46.86 ± 0.74 μg g^{-1} after suspension of the nanoparticles at a concentration of 100 μg mL^{-1}. Then the bulk solution phase levels rise further to 50.24 ± 0.34 μg g^{-1} over 4 hours, shown in Figure 2. The sudden increase in dissolved Zn^{2+} in the minimal salts medium from the measured background concentration may be attributed to the rapid dissolution of small nanoparticles in the large size distribution with the larger nanoparticles dissolving more slowly. After 4 hours the total Zn^{2+} concentration in the bulk solution phase fell slightly, within the confidence limits of the measurements indicating a Zn^{2+} sink in the system.

Measurements of *E. coli* replication in the minimal salts medium, in the dark and with ZnO nanoparticles show the effect of increasing Zn^{2+} concentration in solution. The nanoparticles are found to reduce the replication rate as shown in Figure 3(a). The growth response of *E. coli* to the concentration of Zn^{2+} derived from the ZnO nanoparticles appears to be greater than that to the bulk Zn^{2+} derived from the metal chloride: ZnO nanoparticles are more than just a source of Zn^{2+} Figure 3(b). The differential ZnO nanoparticle-$ZnCl_2$

growth effect on the *E. coli* was also observed at the transcriptional level by measuring the levels of Zn^{2+}-induced transcription of genes encoding di-valent metal ion transporters on the *E. coli* genome in the dark using real-time PCR. The *zntA* gene encoding a Zn^{2+} efflux protein and the *znuC* gene encoding a subunit of a Zn^{2+} import protein were regulated to greater levels after 10 minutes following exposure to ZnO nanoparticles than after exposure to the same bulk solution concentration of Zn^{2+}, added as $ZnCl_2$, Figure 4, although the effects are small.

Subsequently we investigated the photo-toxic mechanism of ZnO nanoparticle anti-bacterial activity and toxicity. The UV-Visible extinction of the ZnO nanoparticle suspensions shows a single feature λ_{max} at approximately 375 nm, (see supporting information, Figure S1) corresponding to the band-gap transition of ZnO and photo-electrons can be produced if the material is irradiated with 375 nm light or shorter wavelengths. The generation of photo-electrons from the nanoparticle in 375 ± 5 nm light was measured using the redox sensitive dye, DCPIP, observed as a colour change at 595 nm, shown in Figure 5. The nanoparticle produces photo-electrons that reduce the DCPIP molecule (with a well defined stoichiometry: one molecule requiring two electrons) causing a first-order exponential decay in the absorbance of the dye with a half-life of 37 minutes. The LEDs used as an UV source produce a total optical output of 5 mW over the wavelength range 375 ± 5 nm. The effects of LED exposure with and without the ZnO nanoparticle photo-centre were measured in suspensions of the bacterium and nanoparticles with an LED mounted in the lid of the culture vessel, covered with aluminium foil. The survival of the bacteria with or without the nanoparticles, and in the light or in the dark over time is shown in Figure 6. There is an accelerating difference between the viability of the *E. coli* with and without the nanoparticles.

The transcriptional-level response of *E. coli* to the photo-electron source was determined by monitoring the regulation of the gene panel by real-time PCR. The expression of the gene panel of redox stress-responsive genes in the *E. coli* was measured 10 minutes after exposure to the ZnO nanoparticles, with or without 375 ± 5 nm light, Figure 7. The panel comprised *soxS*, which is expressed in response to the superoxide radical, *katG*, which is expressed in response to hydrogen peroxide and two superoxide dismutase genes, *sodA* and *sodC*. Primer sequences for real-time PCR reactions are shown in the supporting material. Little or no change in the control experiment (*E. coli* exposed to 375 nm UV) was observed throughout the gene panel but a redox stress response is induced from the presence of ZnO nanoparticles in the dark. However, there is a clear, enhanced up-regulation of *soxS* and *katG* in the presence of ZnO nanoparticles irradiated with the 375 nm UV. Interestingly there is little or no regulation of s*odA and sodC* under any exposure conditions.

Discussion

In this study, the toxic mechanisms of industrial grade, commercially used zinc oxide nanoparticles was tested against the model Gram negative organism, *E. coli* K12, with and without UV irradiation. These conditions differ from those experienced by skin flora in ZnO nanoparticle-based sunscreen where the nanoparticles contain a surface capryl ligand to ensure stability in the oil-based formulation. The oil-based formulation of sunscreens is also significantly different from the current experimental conditions which are intended to test the two toxicity mechanisms of ZnO nanoparticles in the simplest possible medium. Dissolution and photo-radical production in more complex media such as sunscreens or cell culture media represent further experimental challenges but are clearly important concerns for nanotoxicity. ZnO nanoparticles were found to be transiently stable in the minimal salts medium at a pH of 7.2 where the surface charge of the nanoparticles is negative and will be associated with a positive counter-ion shell [41] in the comparatively low ionic strength of the medium. The particle dispersion has a half-life of order hours.

The physical bacterial-nanoparticle interaction was confirmed in TEM image studies of whole *E. coli* that had been exposed to the nanoparticle suspensions, but precluding any disruptive sample preparation, as is typical of standard TEM methods. The cells were washed very gently so as to avoid displacing any associated nanoparticles by placing the specimen grids onto a droplet of glutaraldehyde fixative and then onto sequential drops of water. The images that were obtained do not show any internal detail of the bacteria, Figure 1, but clearly show the nanoparticles as agglomerates on the outer membrane. The primary toxicity structure is therefore large agglomerates of particles of order 1µm in size, which will become covered by any proteins secreted by the bacterium. Some lone particles are seen more intimately interacting with the surface. Dissolution occurs into the nano-bio interface between the nanoparticles and the bacterium which is moderated by the charge on the aggregates and on the negatively charged outer membrane.

The predicted mode of zinc oxide nanoparticle toxicity in the dark is from dissolution and release of toxic zinc ions, Zn^{2+}. The rate of dissolution of zinc oxide nanoparticles was measured in minimal salts medium using ICP-MS. There was a very high initial rate of dissolution consistent with the large particle size distribution: smaller nanoparticles resulting from the gas-phase synthesis are expected to dissolve rapidly. Further, very small nanoparticles are less likely to be removed from solution by the ultracentifugation process even at 50,000 *g* and hence the initial rapid increase in bulk solution phase Zn^{2+} may also be attributed to poor recovery of smaller nanoparticles from the solution before digestions and total Zn^{2+} measurement by ICP-MS. The Zn concentration in the medium increased by approximately 3 µg mL^{-1} over the 4 hour time course, Figure 2. In comparison with other work in our laboratory the same concentration of silver nanoparticles increased the Ag

concentration in the bulk solution phase by 500 ng mL^{-1} over 24 hours, indicating that the ZnO nanomaterial yields a significantly larger concentration of the metal ion.

The ICP-MS data was used to test a differential toxicity hypothesis. This may be stated as the dissolution of a nanoparticle at the bacterial membrane interface may enhance the anti-bacterial efficacy since the nano-bio interface enhances the proximal, interfacial concentration of the Zn^{2+} ions. Thus Zn^{2+} ions are more biologically available than those in the bulk solution. Although the dissolution rate may have been overestimated from nanoparticles that were not removed by the ultracentrifugation there was still a differential effect on *E. coli* growth between the nanoparticles and the measured concentration of Zn^{2+} that they released into the bulk solution, Figure 3. This is consistent with our observations made for silver nanoparticles and observations of a differential nanoparticle-metal ion toxicity reported for fresh water algae [42].

The final experiment to investigate the nanoparticle effects in the dark was to examine a transcriptional profile of the *E. coli* in response to the Zn^{2+} concentration with or without the nanoparticles present. The *E. coli* were cultured with the nanoparticles or Zn^{2+} at a concentration that was determined by the rate of dissolution of the nanoparticles in suspension. A differential level of gene expression was observed; the nanoparticles induced a stronger transcriptional response than the bulk solution phase ions. The bacteria up-regulated the expression of the *zntA* gene (encoding the di-valent metal ion efflux protein), and down-regulated the expression of a gene encoding a di-valent metal ion import protein, Figure 4 within the 10-minute time course of the Real-time PCR experiment. This is consistent with the expected change in the flux of the Zn^{2+} ions across the cell envelope under a state of Zn^{2+} stress; an up-regulation of efflux and a down-regulation of import leading to a net movement of ions out of the cell. If the intensity of the transcriptional response is proportional to the biologically available concentration of the Zn^{2+}, (the ions induce the response when they interact with the Zur and ZntR gene regulatory proteins), these data indicate that the nanoparticles have their enhanced activity by delivering an enhanced biologically available concentration of Zn^{2+}.

The physical-chemical properties of the nano-bio interface can provide additional insight into the dissolution toxicity mechanism. The negatively charged nanoparticles acquire a counter-ion layer that is positively charged although this does not prevent the nanoparticle from dissolving in the electrochemical environment of the minimal salts medium. However, the evidence from the TEM images in Figure 1 show that the nanoparticles and nanoparticle aggregates are associated with the membrane surface of the bacterium which is negatively charged from the lipopolysaccharide components in the outer membrane. On the scale of the nano-bio interface, the electrochemical environment may enhance the dissolution and further concentrate the Zn^{2+} resulting from dissolution at the membrane surface: positively

charged Zn^{2+} is attracted to the negatively charge outer membrane. Enhanced rate of transit across the membrane then produces an enhanced up-regulation of the genes which are known to be subject to femtomolar concentration regulatory control [28]. The transcription-level response occurs following only a ten-minute exposure to the nanoparticles and is clearly the product of a rapid Zn^{2+} release and sensitive homeostasis in *E. coli*.

The suspension of the zinc oxide nanoparticles in the minimal salts medium shows no observable change to the UV-Visible extinction (Figure S1) and hence the photo-excitation associated with the band gap transition. The nanoparticle suspensions absorb UV light including the harmful UVA and UVB radiation [43-45] which is why they are included in sunscreen formulations. Furthermore, as can be inferred from the UV-Visible spectrum of extinction the nanoparticle suspensions absorb little light at visible wavelengths producing colourless or white sunscreens which are cosmetically more desirable. The absorption with λ_{max} at 375 nm represents the band gap of ZnO. This is the minimum energy required to excite a valence band electron into the conduction band and generate photo-electrons, which may reduce redox active species in the medium leading to the production of photo-radicals. For the native particle the high concentration species at the surface is water, and photoelectron production is likely to lead to the formation of the hydroxyl radical which subsequently initiates a radical cascade producing amongst other species, the superoxide radical on collision with dissolved oxygen. The hydroxide radical is the likely progenitor of the radical storm but any radical-labile species in the nano-bio interface will change the radical speciation. This is a key factor in determining the toxicity of commercial formulations for topical application containing ZnO and TiO_2 [45].

The rate of free radical formation was determined using the stoichiometric colour change associated with the $2e^-$ reduction of the redox indicator DCPIP causing a colour change from blue to colourless, Figure 5. The photo-radical assay is limited by the transport of the radical away from the nanoparticle surface to encounter the dye in solution or from the diffusion-limited refreshment of the oxidised dye at the nanoparticle interface replacing the colourless reduced dye. The DCPIP colour change was not observed if the nanoparticles were suspended in the minimal salts medium, indicating that the rate of DCPIP reduction was very slow, or inhibited by the interfacial electrochemistry. DCPIP is not charged and its concentration will not be enhanced in the nano-bio interface which will contain other redox-active species such as Fe^{3+} converting to Fe^{2+} quenching the radical concentration but inducing the redox stress in the bacterium.

In an *E. coli* culture to which the nanoparticles were added, the radicals formed in the nano-bio interface may be delivered directly or indirectly to the metabolism of the bacterium. This direct delivery may be important as radicals clearly have a limited lifetime in solution and once inside the cytoplasm the redox environment will then control the lifetime and

propagate new radicals such as O_2^{2-} and the production of H_2O_2, and lipid peroxides. These are dangerous species for the cell. The radicals may propagate within the cell, particularly through redox cycling of free metal cations including Cu^+ and Fe^{2+}. The predicted intracellular concentration of these free metal ions is higher in the nanoparticle treated *E. coli* whereby the dissolution and concentration of free Zn^{2+} may displace these ions from their coordination sites with proteins. The free radical damage to membrane lipids, proteins and DNA contribute to the loss of cell viability as observed in Figure 6. Their concentration within the bacterium will be combated by the redox stress response [40], which was determined from the transcription of redox-stress associated genes, Figure 7.

Two genes, *katG* and *soxS*, which are up-regulated following the activation of the *soxRS* and *oxyR* (redox stress-responding) regulons showed a response to the presence of the nanoparticles in 375 nm light. Oxidation of the SoxR sensor, through the [2Fe–2S], initiates the regulation. There is some uncertainty about the nature of the cellular signal that is sensed [46], the iron sulphur components are vulnerable to redox electrochemistry and many factors may trigger up regulation. Similar triggers may occur from other iron-containing regulators [47] in response to the changed redox conditions. This is supported by the *E. coli* transcriptional response at a reduced level in the dark. This UV-independent response may represent the disruption of metal ion coordination sites by the excess Zn^{2+}, thus leading to an increase in free copper and iron without photo-radical initiation. It has been shown recently that superoxide is not the only signal that SoxR senses [48] and other photo-radicals formed initially at the nano-bio interface, perhaps OH or methy radicals, or even reduction of Zn^{2+} to zinc atoms in the dissolution plume, change the electrochemical balance and trigger the redox stress response in only ten minutes.

The lack of superoxide in the nano-bio interface is indicated directly the lack of regulation of the gens *sodA* and *sodC*. These superoxide dismutase encoding genes surprisingly did not show any regulation following exposure to the nanoparticles, either in the dark or under UV light. The *sodA* gene is positively regulated by *soxS*, however another level of regulation for this gene must exist such that it was not transcribed even though *soxS* was expressed at high levels. In contrast the *sodC* gene is regulated by the *rpoS* sigma, associated with stationary phase.

In conclusion, two experimental studies point directly at a zinc nanoparticle dissolution toxicity and a photo-radical induced redox stress toxicity in *E. coil.* Both mechanisms are significantly modified by the structure of the nano-bio interface with interfacial concentration enhancements of Zn^{2+} producing a larger Zn^{2+} regulatory response for the nanoparticle delivery mechanism. The second photo-radical mechanism did not produce the expected superoxide radicals that survive the passage into the cell to trigger the regulation of the superoxide dismutase genes. There was also not formation of radical

species in the minimal salts medium preventing the photo-reduction of the DCPIP dye. In this mechanism, the nano-bio interface modifies the radical storm producing an enhanced redox stress response almost certainly from oxidation state changes in metal ions such as Cu^{+}/Cu^{2+}, Fe^{2+}/Fe^{3+} redox couples. In addition, this study demonstrates speciation in nanoparticle toxicity to include a 'whole nanoparticle' effect wherein the photo-activation of the ZnO surfaces leads to redox stress in the *E. coli* metabolism. The formation of free radicals is considered to contribute to cellular damage by a variety of mechanisms. One of these is the degradation of DNA, potentially leading to gene mutation. This may have considerable implications for the use of these nanoparticles as topical preparations that are spread on the skin and in the aquatic environment. Topical application studies demonstrate how these nanomaterials may not cross the outermost layer of skin, the stratum corneum, thus the underlying epidermis may be protected from their effects [49]. However, the skin surface is covered with an immunologically important normal skin flora [50] which will be subject to both nanotoxicity mechanisms; dissolution and photo-electron effects. Application of ZnO-containing formulations to the skin surface may have a considerable impact these organisms. This in turn may leave the host open to the carriage of pathogenic species where the normal flora organisms restrict the colonisation of the skin by occupying each environmental niche on the skin surface, colonisation resistance [51].

Acknowledgements

JM would like to thank the BBSRC for a CASE award with ENBL Ltd. We would like to thanks Dr Sara Burton and Prof Hilary Lapin-Scott for their support during the early parts of this work. We would like to thank Dr Heidi Groenaga Infante and Dr Volker Nischwitz at the Laboratory of the Government Chemist for ICP-MS measurements.

References

1. Klingshirn, C., *ZnO: material, physics and applications.* Chemphyschem, 2007. **8**(6): p. 782-803.
2. Nadanathangam, V. and et al., *Functional finishing of cotton fabrics using zinc oxideâ€"soluble starch nanocomposites.* Nanotechnology, 2006. **17**(20): p. 5087.
3. Aydin Sevinç, B. and L. Hanley, *Antibacterial activity of dental composites containing zinc oxide nanoparticles.* Journal of Biomedical Materials Research Part B: Applied Biomaterials, 2010. **94B**(1): p. 22-31.
4. Boyd, D., et al., *The antibacterial effects of zinc ion migration from zinc-based glass polyalkenoate cements.* Journal of Materials Science: Materials in Medicine, 2006. **17**(6): p. 489-494.
5. Moorer, W.R. and J.M. Genet, *Evidence for antibacterial activity of endodontic gutta-percha cones.* Oral Surgery, Oral Medicine, Oral Pathology, 1982. **53**(5): p. 503-507.
6. Brayner, R., et al., *Toxicological Impact Studies Based on Escherichia coli Bacteria in Ultrafine ZnO Nanoparticles Colloidal Medium.* Nano Letters, 2006. **6**(4): p. 866-870.
7. Hu, X., et al., *In vitro evaluation of cytotoxicity of engineered metal oxide nanoparticles.* Science of The Total Environment, 2009. **407**(8): p. 3070-3072.
8. Huang, Z., et al., *Toxicological Effect of ZnO Nanoparticles Based on Bacteria.* Langmuir, 2008. **24**(8): p. 4140-4144.
9. Jiang, W., H. Mashayekhi, and B. Xing, *Bacterial toxicity comparison between nano- and micro-scaled oxide particles.* Environmental Pollution, 2009. **157**(5): p. 1619-1625.
10. Li, X., et al., *Antimicrobial activities of ZnO powder-coated PVC film to inactivate food pathogens.* International Journal of Food Science & Technology, 2009. **44**(11): p. 2161-2168.
11. Reddy, K.M., et al., *Selective toxicity of zinc oxide nanoparticles to prokaryotic and eukaryotic systems.* Appl Phys Lett, 2007. **90**(213902): p. 2139021-2139023.
12. Zhang, L., et al., *Investigation into the antibacterial behaviour of suspensions of ZnO nanoparticles (ZnO nanofluids).* Journal of Nanoparticle Research, 2007. **9**(3): p. 479-489.
13. Nel, A.E., et al., *Understanding biophysicochemical interactions at the nano-bio interface.* Nat Mater, 2009. **8**(7): p. 543-557.
14. Auld, D.S., *Zinc coordination sphere in biochemical zinc sites.* BioMetals, 2001. **14**(3): p. 271-313.
15. Vallee, B.L. and D.S. Auld, *Active zinc binding sites of zinc metalloenzymes.* Matrix Suppl, 1992. **1**: p. 5-19.
16. Vallee, B.L. and D.S. Auld, *Functional zinc-binding motifs in enzymes and DNA-binding proteins.* Faraday Discuss, 1992(93): p. 47-65.
17. Christianson, D.W., *Structural biology of zinc.* Adv Protein Chem, 1991. **42**: p. 281-355.
18. Vallee, B.L. and D.S. Auld, *Zinc coordination, function, and structure of zinc enzymes and other proteins.* Biochemistry, 1990. **29**(24): p. 5647-59.
19. Coleman, J.E., *Zinc proteins: enzymes, storage proteins, transcription factors, and replication proteins.* Annu Rev Biochem, 1992. **61**: p. 897-946.
20. Katayama, A., et al., *Systematic search for zinc-binding proteins in Escherichia coli.* European Journal of Biochemistry, 2002. **269**(9): p. 2403-2413.
21. Daneshvar, N., D. Salari, and A.R. Khataee, *Photocatalytic degradation of azo dye acid red 14 in water on ZnO as an alternative catalyst to TiO2.* Journal of Photochemistry and Photobiology A: Chemistry, 2004. **162**(2-3): p. 317-322.
22. Wang, C., et al., *Enhanced photocatalytic performance of nanosized coupled ZnO/SnO2 photocatalysts for methyl orange degradation.* Journal of Photochemistry and Photobiology A: Chemistry, 2004. **168**(1-2): p. 47-52.

23. Jang, Y.J., C. Simer, and T. Ohm, *Comparison of zinc oxide nanoparticles and its nano-crystalline particles on the photocatalytic degradation of methylene blue.* Materials Research Bulletin, 2006. **41**(1): p. 67-77.
24. Gulson, B., et al., *Small amounts of zinc from zinc oxide particles in sunscreens applied outdoors are absorbed through human skin.* Toxicological Sciences, 2010.
25. Davidson, A.L., et al., *Structure, Function, and Evolution of Bacterial ATP-Binding Cassette Systems.* Microbiol. Mol. Biol. Rev., 2008. **72**(2): p. 317-364.
26. Patzer, S.I. and K. Hantke, *The ZnuABC high-affinity zinc uptake system and its regulator Zur in Escherichia coli.* Molecular Microbiology, 1998. **28**(6): p. 1199-1210.
27. Grass, G., et al., *ZupT Is a Zn(II) Uptake System in Escherichia coli.* J. Bacteriol., 2002. **184**(3): p. 864-866.
28. Outten, C.E. and T.V. O'Halloran, *Femtomolar sensitivity of metalloregulatory proteins controlling zinc homeostasis.* Science, 2001. **292**(5526): p. 2488-92.
29. Patzer, S.I. and K. Hantke, *The zinc-responsive regulator Zur and its control of the znu gene cluster encoding the ZnuABC zinc uptake system in Escherichia coli.* J Biol Chem, 2000. **275**(32): p. 24321-32.
30. Grass, G., et al., *ZitB (YbgR), a Member of the Cation Diffusion Facilitator Family, Is an Additional Zinc Transporter in Escherichia coli.* J. Bacteriol., 2001. **183**(15): p. 4664-4667.
31. Rensing, C., B. Mitra, and B.P. Rosen, *The zntA gene of Escherichia coli encodes a Zn(II)-translocating P-type ATPase.* Proc Natl Acad Sci U S A, 1997. **94**(26): p. 14326-31.
32. Beard, S.J., et al., *Zinc(II) tolerance in Escherichia coli K-12: evidence that the zntA gene (o732) encodes a cation transport ATPase.* Mol Microbiol, 1997. **25**(5): p. 883-91.
33. Blencowe, D.K. and A.P. Morby, *Zn(II) metabolism in prokaryotes.* FEMS Microbiology Reviews, 2003. **27**(2-3): p. 291-311.
34. Binet, M.R. and R.K. Poole, *Cd(II), Pb(II) and Zn(II) ions regulate expression of the metal-transporting P-type ATPase ZntA in Escherichia coli.* FEBS Lett, 2000. **473**(1): p. 67-70.
35. Brocklehurst, K.R., et al., *ZntR is a Zn(II)-responsive MerR-like transcriptional regulator of zntA in Escherichia coli.* Mol Microbiol, 1999. **31**(3): p. 893-902.
36. Outten, C.E., F.W. Outten, and T.V. O'Halloran, *DNA distortion mechanism for transcriptional activation by ZntR, a Zn(II)-responsive MerR homologue in Escherichia coli.* J Biol Chem, 1999. **274**(53): p. 37517-24.
37. Choi, H., et al., *Structural basis of the redox switch in the OxyR transcription factor.* Cell, 2001. **105**(1): p. 103-13.
38. Zheng, M., F. Aslund, and G. Storz, *Activation of the OxyR transcription factor by reversible disulfide bond formation.* Science, 1998. **279**(5357): p. 1718-21.
39. Singh, R., et al., *Comparative study of catalase-peroxidases (KatGs).* Archives of Biochemistry and Biophysics, 2008. **471**(2): p. 207-214.
40. Demple, B., *Radical ideas: genetic responses to oxidative stress.* Clin Exp Pharmacol Physiol, 1999. **26**(1): p. 64-8.
41. Walker, N., *Personal Communication*. 2010.
42. Navarro, E., et al., *Toxicity of Silver Nanoparticles to Chlamydomonas reinhardtii.* Environmental Science & Technology, 2008. **42**(23): p. 8959-8964.
43. Becheri, A., et al., *Synthesis and characterization of zinc oxide nanoparticles: application to textiles as UV-absorbers.* Journal of Nanoparticle Research, 2008. **10**(4): p. 679-689.
44. Marissa, D.N., S. Mira, and I.E. Jeffrey, *The safety of nanosized particles in titanium dioxideâ€“ and zinc oxideâ€“based sunscreens.* Journal of the American Academy of Dermatology, 2009. **61**(4): p. 685-692.
45. Nohynek, G.J., et al., *Grey Goo on the Skin? Nanotechnology, Cosmetic and Sunscreen Safety.* Critical Reviews in Toxicology, 2007. **37**(3): p. 251-277.

46. Krapp, A.R., M.V. Humbert, and N. Carrillo, *The soxRS response of Escherichia coli can be induced in the absence of oxidative stress and oxygen by modulation of NADPH content.* Microbiology, 2011. **157**(4): p. 957-965.
47. Fleischhacker, A.S. and P.J. Kiley, *Iron-containing transcription factors and their roles as sensors.* Current Opinion in Chemical Biology, 2011. **15**(2): p. 335-341.
48. Gu, M. and J.A. Imlay, *The SoxRS response of Escherichia coli is directly activated by redox-cycling drugs rather than by superoxide.* Molecular Microbiology, 2011. **79**(5): p. 1136-1150.
49. Gamer, A.O., E. Leibold, and B. van Ravenzwaay, *The in vitro absorption of microfine zinc oxide and titanium dioxide through porcine skin.* Toxicology in Vitro, 2006. **20**(3): p. 301-307.
50. Gao, Z., et al., *Molecular analysis of human forearm superficial skin bacterial biota.* Proceedings of the National Academy of Sciences, 2007. **104**(8): p. 2927-2932.
51. Noble, W.C., *The Skin Microflora and Microbial Skin Disease*. 1993: Cambridge University Press.

Figure captions

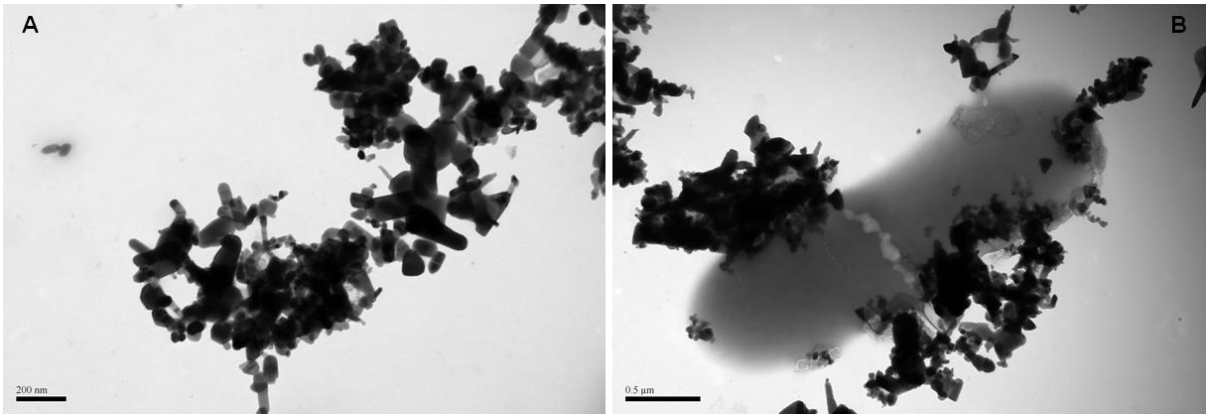

Figure 1. Transmission electron micrograph of the ZnO nanoparticles after suspension in the minimal salts medium (A) and *E. coli* bacteria after mixing with the ZnO nanoparticle suspension in the minimal salts medium (B).

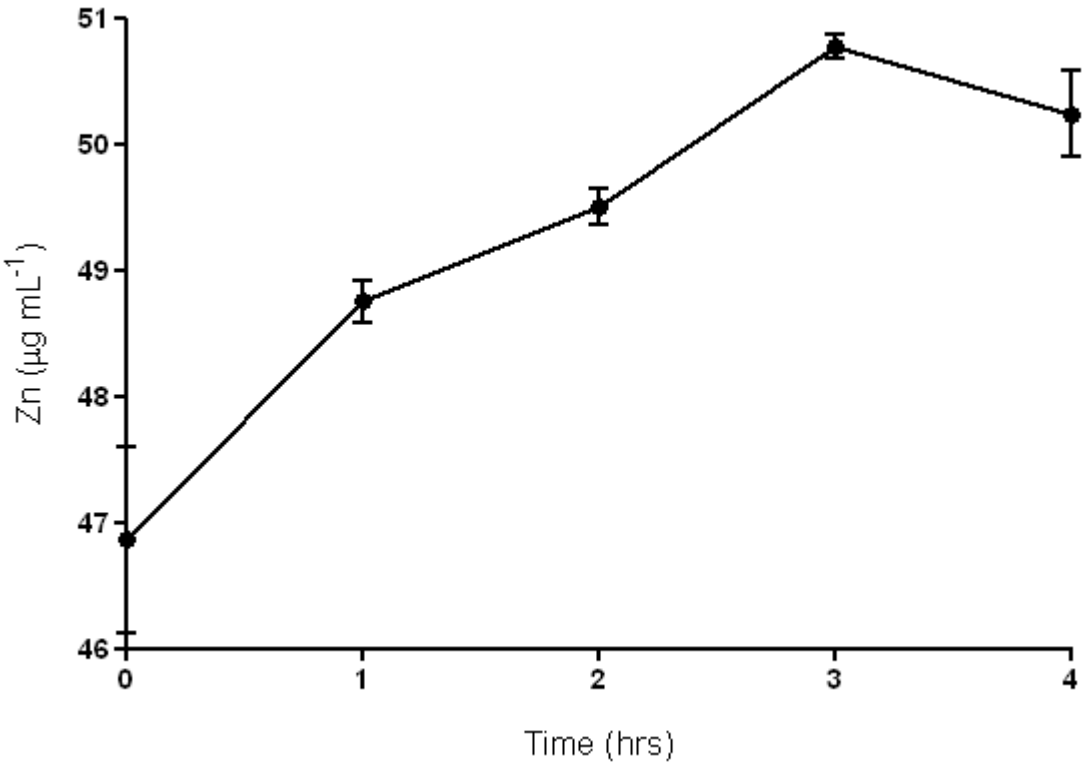

Figure 2. Dissolution of 100 µg mL $^{-1}$ of the ZnO nanoparticles in the minimal salts medium. The bulk solution phase Zn at each time point was determined by removing the nanoparticles from a sample of the medium using ultracentrifugation and measuring total Zn in the supernatant by ICP-MS.

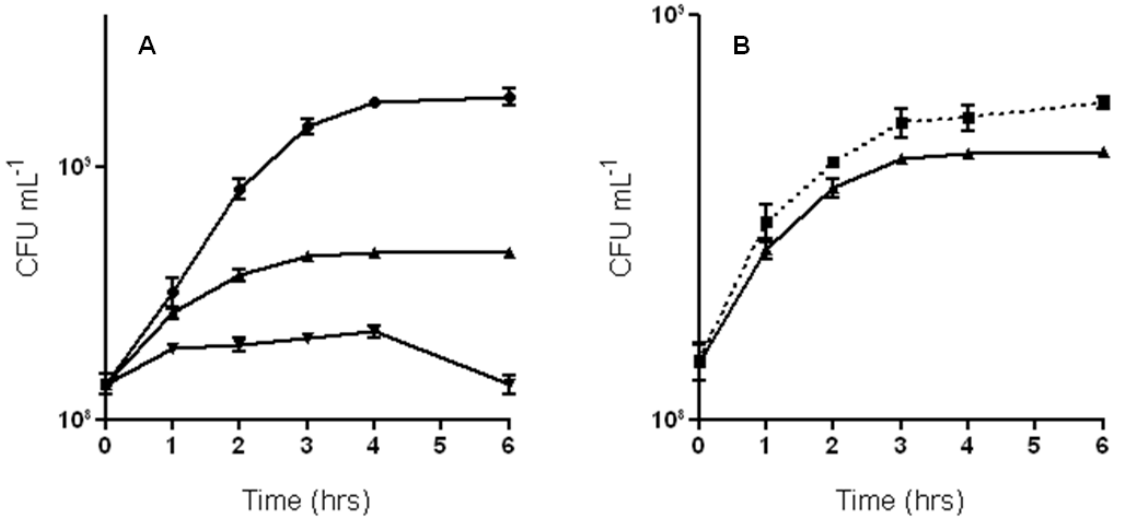

Figure 3. (A) Growth curves for *E. coli* in the minimal salts medium; native growth curve (●), growth in a suspension of 100 µg mL $^{-1}$ of the ZnO nanoparticles (▲) and growth in a suspension of 200 µg mL $^{-1}$ of the ZnO nanoparticles (▼). (B) Growth curves for *E. coli* in the medium containing ZnO nanoparticles (■) or zinc chloride added at the rate of nanoparticle dissolution (▲). Error bars are the standard error of the mean (n=3).

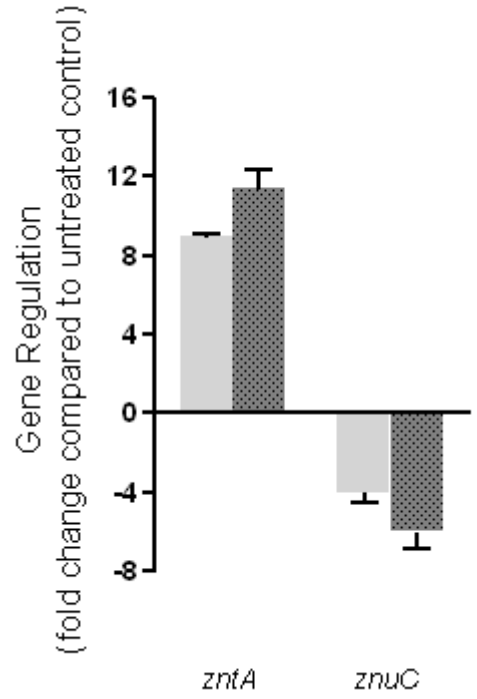

Figure 4. Regulation of Zn^{2+}-responsive genes was measured by real-time PCR. The *zntA* gene encodes a Zn^{2+} efflux protein and is induced by zinc. The *znuC* gene encodes a sub-unit of a Zn^{2+} import protein and is repressed by zinc. Gene regulation was measured after exposure for 10 minutes to 100 µg mL $^{-1}$ of the ZnO nanoparticles (light grey bars) or 50 µg mL $^{-1}$ of Zn^{2+} as zinc chloride, corresponding to the measured bulk solution phase Zn from

the nanoparticles (dark grey, shaded bars). The reported values are relative to an untreated control. The error bars are the standard error of the mean (*n*=3).

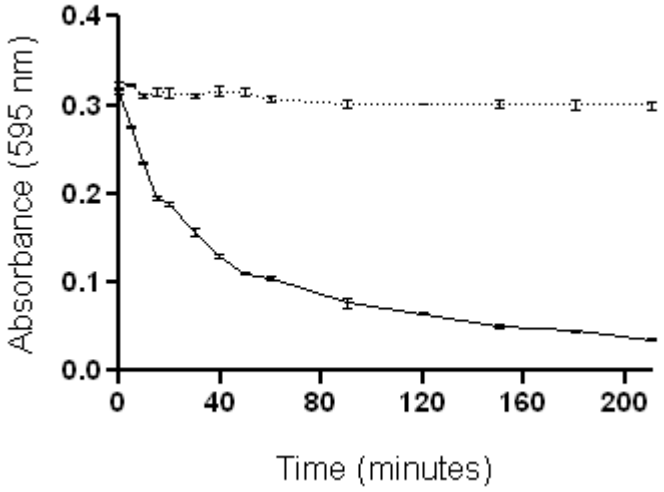

Figure 5. Colour change as measured by absorbance at 595 nm of the redox sensitive dye, DCPIP. With 100 µg mL $^{-1}$ of the ZnO nanoparticles suspended in the minimal salts medium in the dark (dotted line) or in 375 nm light (solid line). Error bars are the standard error of the mean (*n*=3).

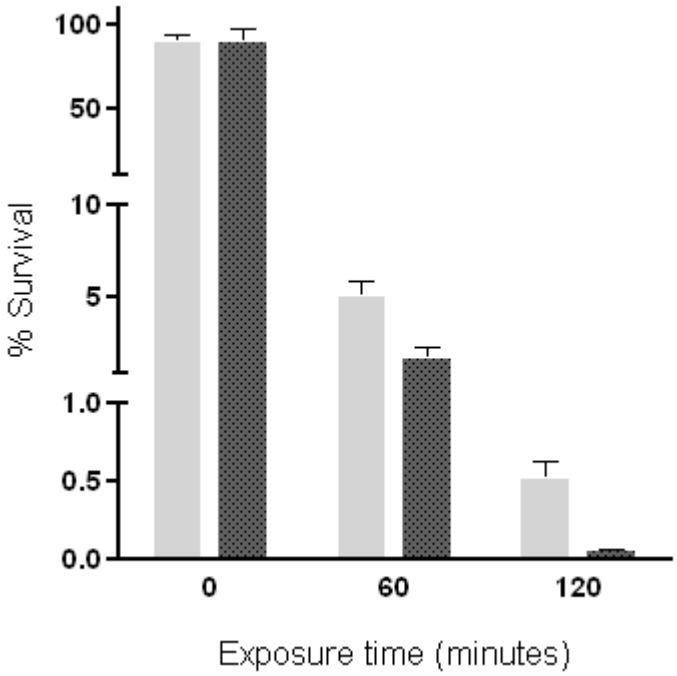

Figure 6. Survival of *E. coli* in a suspension of 100 µg mL $^{-1}$ of the ZnO nanoparticles in water, in the dark (light grey bars) or in 375 nm light (dark grey shaded bars). The error bars are the standard error of the mean (n=3).

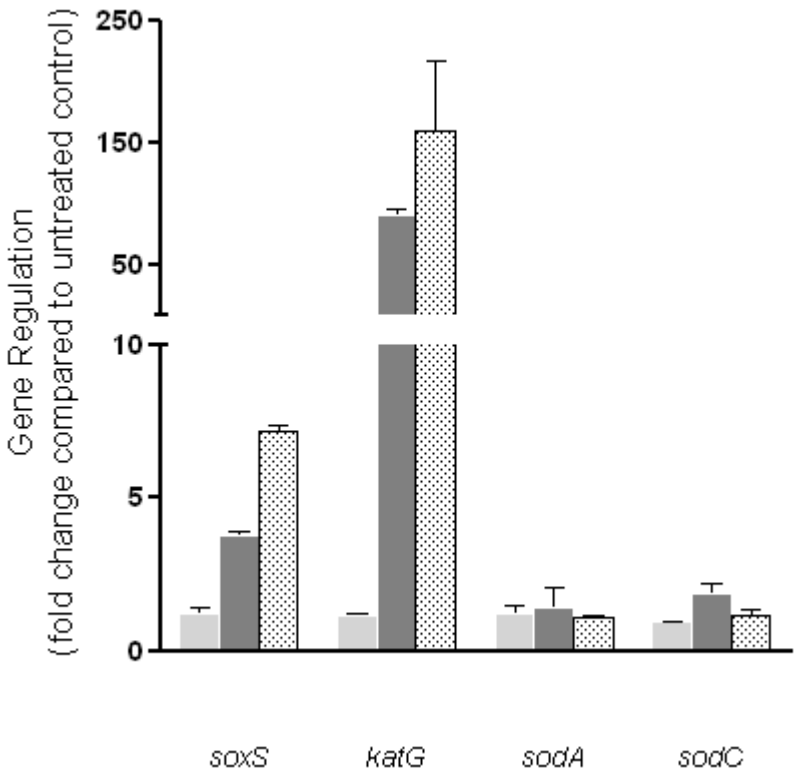

Figure 7. Regulation of radical-responsive genes was measured by real-time PCR. Gene regulation was measured after exposure to 375 nm light (light grey bars) or to 100 µg mL $^{-1}$ of the ZnO nanoparticles (dark grey bars) or to 100 µg mL $^{-1}$ of the ZnO nanoparticles and 375 nm light (shaded bars), all relative to untreated controls. All exposures were for 10 minutes. The reported values are relative to an untreated control. The error bars are the standard error of the mean (*n*=3).

Supplementary figure captions

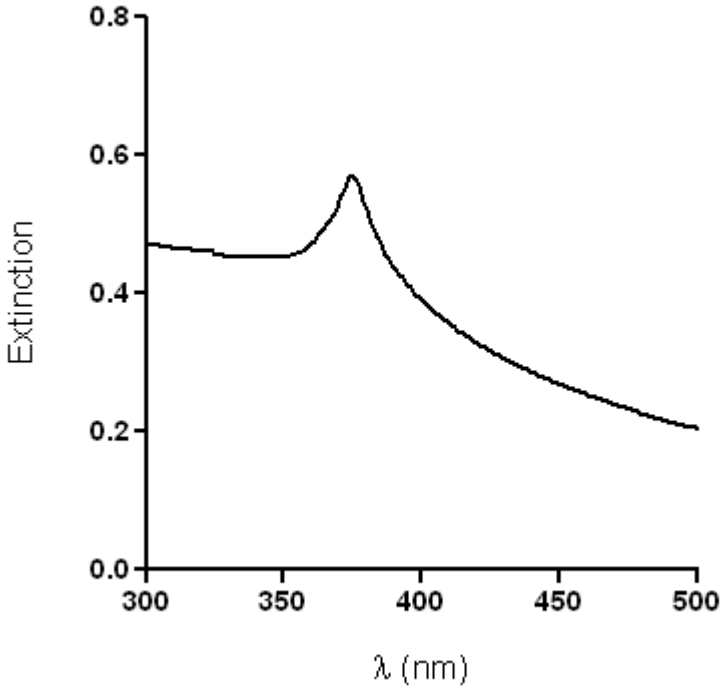

Figure S1. UV-visible extinction spectrum of 100 µg mL-1 of the ZnO nanoparticles in the minimal salts medium.

Supplementary tables

Table S1. Oligonucleotide primers used in the Real-Time PCR analysis.

Target	Forward Sequence (5' - 3')	Reverse Sequence (5' - 3')
zntA	GGAAGAGGTGGCGATTAACA	TTCTGACAGCACTTCCAACG
znuC	GATGAAGTGCTGTGCCTGAA	GCAAAACAATTCGTCCCTGT
soxS	GTAATCGCCAAGCGTCTGAT	CCCATCAGAAAATTATTCAGGATCT
katG	CAACCGAGATGGGTCTGATT	TTGTTCTTCAATCGGTGCAG
sodA	GGAAATCCACCACACCAAAC	GATAGCCGCTTTCAGGTCAC
sodC	TCTGGCCCTTCATGTTTACC	GCAGTCAATTGGTAGCGTCA
rrsB	CAGCCACACTGGAACTGAGA	GTTAGCCGGTGCTTCTTCTG